FINITE ELEMENT SIMULATION OF A GRADIENT ELASTIC HALF-SPACE SUBJECTED TO THERMAL SHOCK ON THE BOUNDARY

[1]Theodosios K. Papathanasiou, [2]Panos A. Gourgiotis, [3]Francesco Dal Corso

DICAM, University of Trento, I-38123, Trento, Italy.

[1]e-mail: t.papathanasiou@unitn.it

[2]e-mail: p.gourgiotis@unitn.it

[3]e-mail: francesco.dalcorso@unitn.it

Abstract. The influence of the microstructure on the macroscopical behavior of complex materials is disclosed under thermal shock conditions. The thermal shock response of an elastic half-space subjected to convective heat transfer at its free surface from a fluid undergoing a sudden change of its temperature is investigated within the context of the generalized continuum theory of gradient thermoelasticity. This theory is employed to model effectively the material microstructure. This is a demanding initial boundary value problem which is solved numerically using a higher-order finite element procedure. Simulations have been performed for different values of the microstructural parameters showing that within the gradient material the thermoelastic pulses are found to be dispersive and smoother than those within a classical elastic solid, for which the solution is retrieved as a special case. Energy type stability estimates for the weak solution have been obtained for both the fully and weakly coupled thermoelastic systems. The convergence characteristics of the proposed finite element schemes have been verified by several numerical experiments. In addition to the direct applicative significance of the obtained results, our solution serves as a useful benchmark for modeling more complicated problems within the framework of gradient thermoelasticity.

Keywords: Thermoelasticity, gradient elasticity, micro-inertia, microstructure, stability estimates, transient effects

1. Introduction

It is well-known that the material microstructure influences the macroscopical behavior of complex solids, such as composites, cellular materials, and ceramics. Classical continuum theories do not incorporate internal length-scales and therefore cannot capture the pertinent scale effects that are associated with the underlying material microstructure. To this purpose, various generalized (enhanced) continuum theories (for a comprehensive review, see [1]) have been proposed, enriching the classical description with additional material length scales and, thus, extending the range of applicability of the 'continuum' concept in an effort to bridge the gap between classical continuum theories and atomic-lattice theories. These models have also been derived from the theoretical identification of homogeneous materials equivalent to composites with heterogeneous classic phases [2-5] and from experimental testing at small scales [6-8].

In the last decade, the study of microstructured materials through enhanced continuum theories has been significantly boosted by recent advances in the fields of nanomechanics, micromachining, and bioengineering. The use of such theories allows a more accurate description of the mechanical response of high performance microstructured materials for instance, in problems where high strain / stress gradients emerge [9-12] or when instability phenomena are involved [13-15].

One of the most effective generalized continuum theories has proved to be the theory of gradient elasticity, also known as dipolar gradient elasticity or grade-two theory [16, 17]. According to the gradient elasticity theory, the material points inside a continuum can be visualized as micro-continuum with their own internal displacement field described in reference to a local coordinate system. Assuming enough regularity of the deformation process, the internal displacement field of each point can be expanded in Taylor series. If only the linear terms of these expansions are retained, the dipolar theory is obtained. The continuum under consideration consists of structural units (micro-media) in the form of cubes with edge length, which is an inherent length characteristic of the material structure (e.g. grain size). The presence of this length parameter, in turn, implies that the gradient elasticity theory encompasses the analytical possibility of size effects, which are absent in the classical theory. The physical relevance of the characteristic material length scales as introduced through gradient type theories has been the subject of numerous experimental studies. In particular, atomistic calculations and experiments indicate that for most metals, the characteristic internal length is of the order of the lattice parameter [4, 18]. However, foam and cellular materials exhibit a characteristic length that is comparable to the average cell size, whereas in laminates is of the order of the laminate thickness [2,7,8].

In recent years, the thermoelastic behavior of complex microstructured materials has attracted considerable attention since their high performance properties are closely related to their reliability under changing thermal conditions. Various gradient type models have been developed in order to describe the thermomechanical response of

such microstructured continua [19-24]. In several of these models non-local phenomena in the time dependence of the fields have been also considered, leading to non-Fourier heat transfer models like the Vernotte-Cattaneo model [25, 26]. The generalized Green-Lindsay model presented in [23], in a reduced form corresponding to the consideration of classical Fourier heat diffusion, will be the subject of the present analysis. This particular model will be employed for the study of the response of a gradient elastic half-space subjected to thermal shock on its boundary. The thermal shock is induced by convective heat transfer with a surrounding medium that undergoes a sudden change in its temperature (Fig. 1). The problem examined in the present work extends the analysis of Danilovskaya [27] to a microstructured material modelled by gradient thermoelasticity. The goal of the present study is to reveal the influence of the microstructure on the macroscopical behavior of complex materials under thermal shock conditions. It is worth noting that due to the complexity of the equations of gradient thermoelasticity very few solutions to benchmark initial-boundary problems, such as the present one, exist in the literature.

The paper is organized as follows. The equations governing the thermoelastic response of a gradient elastic solid, as derived in [23], are briefly introduced. After selecting appropriate nondimensional quantities, the respective Initial-Boundary Value Problem (IBVP) is stated. The variational form of the problem is defined and stability estimates for the weak solution are provided. Both cases of weak and strong thermoelastic coupling are analyzed. The case of a classical thermoelastic half-space may be retrieved by setting the microstructural parameters of the enhanced model to zero. In the framework of classical elasticity, the problem under consideration has been treated by many authors [27-31], and these results will be used as reference solutions for comparison between the two theories.

For the solution of the enhanced thermoelastic model, special finite elements are introduced, based on the weak formulation of the IBVP. These 3 node elements feature Hermite polynomials of 5^{th} degree for the approximation of the displacement field. The higher regularity finite element space introduced is needed due to the higher order spatial derivatives acting on the displacement field in the governing partial differential equations. Several numerical results are presented and the convergence characteristics of the proposed numerical scheme are studied in detail. An energy balance equation is formulated based on the variational form of the weakly coupled system and the compliance of the numerical solutions with this constraint is analyzed. Moreover, the dispersive nature of the thermoelastic pulses, as dictated by the gradient elasticity theory [32-35], has been verified and found to occur in normal or anomalous type, depending on the relative magnitude of the microstructural parameters. It is shown that the resulting kinematic fields (displacements, strains) are smoother than those predicted by the classical theory of thermoelasticity [31].

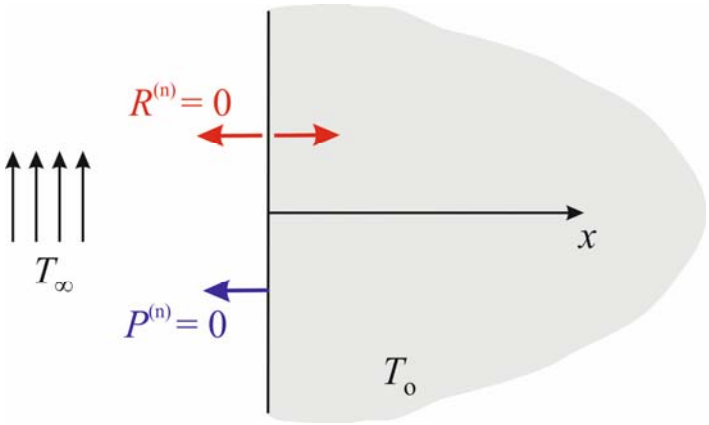

Figure 1. Gradient elastic half-space subjected to convective heat transfer with a surrounding fluid at its free boundary.

2. Governing Equations

In the following, we consider a homogeneous gradient elastic half space. The half-space is assumed to be initially at uniform temperature T_o and the free surface is suddenly subjected to convection heat transfer with a surrounding fluid medium at temperature $T_\infty > T_o$. The convective heat transfer starts at time instant $t=0$ and constitutes the only forcing for all $t>0$. The governing equations for the thermoelastic response of a solid have been derived in the framework of gradient elasticity theory as a special case of more general thermoelastic models [23, 24] including second sound effects for the heat diffusion phenomenon. In what follows, we assume classical Fourier heat transfer. Since the convection boundary condition is applied uniformly on the free surface of the half-space, the temperature and displacement field vary only in the direction x along the depth of the half-space. Assuming that at point x and time instant t, the temperature inside the half-space is $T(x,t)$, we introduce the temperature difference $\theta(x,t)=T(x,t)-T_o$. For small values of the temperature variation θ, the three dimensional classical thermoelastic equations for a gradient elastic solid (see e.g. [23]) are reduced to the following 1D system

$$\rho c_e \theta_t - k\theta_{xx} + T_o a(3\lambda+2\mu)u_{xt} = 0 \quad , \tag{1}$$

$$\rho u_{tt} - 3^{-1}\rho H^2 u_{xxtt} - (\lambda+2\mu)\left(u - g^2 u_{xx}\right)_{xx} + a(3\lambda+2\mu)\theta_x = 0 \, . \tag{2}$$

where u is the displacement along the x - axis and ρ, c_e, k, a are the material density, specific heat capacity under constant strain, thermal conductivity and thermal expansion coefficient respectively. The classical notation λ, μ is used for the Lamé constants of elasticity. Moreover, the subscripts x, t denote differentiation with respect

to the spatial and temporal variable, respectively. Finally, the characteristic lengths associated with gradient elasticity are H and g, providing higher order contributions to the kinetic and strain energy densities respectively.

Appropriate boundary conditions, variationally consistent with (2), at the traction-free surface of the half-space are [16, 17]

$$P^{(n)}=0\Rightarrow 3^{-1}\rho H^2 u_{xtt}+(\lambda+2\mu)(u_x-g^2u_{xxx})-a(3\lambda+2\mu)\theta=0\text{, on } x=0\text{,} \quad (3a)$$

$$R^{(n)}=0\Rightarrow u_{xx}=0\text{, on } x=0\text{,} \quad (3b)$$

expressing zero monopolar $P^{(n)}$ and dipolar $R^{(n)}$ tractions, respectively. Note that the dipolar traction $R^{(n)}$ represents a double-stress without a moment (pinch). An example from structural mechanics of similar self-equilibrating double-forces without moment can be found in the bending analysis of a beam with T-type cross-section [36]. Moreover, the monopolar traction $P^{(n)}$ represents the force-vector acted upon the free surface.

The following point now deserves attention: in the general dynamical case, the existence of the inertia and micro-inertia terms in the equation of motion and in the boundary conditions (see Eqs. (2) and (3a)) violates the assumption of (Euclidean) objectivity when the motion is considered in non-inertial frames. As Jaunzemis [37, p. 233] points out, the issue of objectivity in constrained generalized continuum theories (e.g. constrained Cosserat and strain-gradient theories) can be circumvented by introducing an objective generalized (effective) body force and an objective generalized body double-force. The former is defined as the difference of the standard body force and the inertia term (related to the acceleration – see also [38, p. 159] in the classical setting), and the latter as the difference of the standard body double-force and the micro-inertia term (related to the acceleration gradient). The generalized body force and body double-force are assumed to be objective although its constituents are not (see also [39]).

The convection heat transfer occurring at $x=0$ is expressed through Newton's law of cooling as

$$k\theta_x=C_c\left(\theta-\theta_\infty\right)\text{, where } \theta_\infty=T_o-T_\infty\text{.} \quad (4)$$

where C_c is the convection coefficient. The surrounding fluid medium temperature θ_∞ is assumed to be a function of the temporal variable with the form

$$\theta_\infty(t)=\Phi\, f(t)\text{,} \quad (5)$$

where Φ is the temperature increase or decrease, with respect to the reference state T_o, attained by the surrounding medium and $f(t):[0,\bar{J}]\rightarrow[0,1]$, is a function

characterizing the temperature forcing variation with respect to time. For the classical 'thermal shock' condition it is $f(t)=\mathcal{H}(t-t_0)$, where $\mathcal{H}$ denotes the Heaviside function. Mollified versions of thermal shock conditions may be also modeled by selecting appropriately the form of f (e.g. ramp functions) as shown in figure 2.

At infinity, vanishing temperature, displacement and displacement gradient fields are assumed

$$\lim_{x\to\infty}\{\theta,u,u_x\}=0, \tag{6}$$

while zero initial conditions are imposed as

$$\theta(x,0)=u(x,0)=u_t(x,0)=0. \tag{7}$$

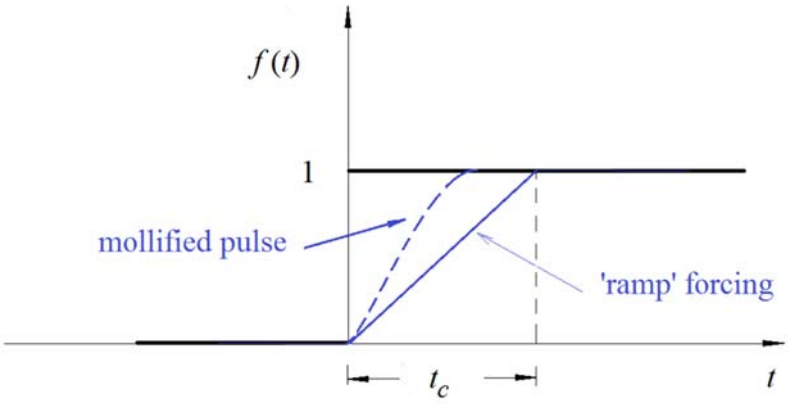

Figure 2. Time profile of the temperature change in the surrounding fluid, influencing convective heat transfer with the gradient elastic half-space.

3. Nondimensional quantities and scaling considerations

Let us introduce the thermal diffusivity $\kappa=k/(\rho c_e)$ and the elastic P-wave speed $c_p=\sqrt{(\lambda+2\mu)/\rho}$. The characteristic length for the classical thermoelastic model is $\varepsilon=\kappa/c_p$. Utilizing these parameters, the following nondimensional quantities are introduced

$$\xi=x/\varepsilon\ ,\ \eta=c_p t/\varepsilon\ ,\ \Theta=\theta/T_o\ ,\ U=u/\varepsilon. \tag{8}$$

Let $J=c_p\bar{J}/\varepsilon\in\mathbb{R}_+$ and set $Q\doteq(0,J)\times(0,\infty)$. The initial – boundary value (IBVP) problem in nondimensional form becomes: Find Θ, U such that

$$\Theta_\eta-\Theta_{\xi\xi}+D_1U_{\xi\eta}=0, \text{ in } Q \tag{9}$$

$$U_{\eta\eta} - \lambda_A^2 U_{\xi\xi\eta\eta} - \left(U_\xi - \lambda_B^2 U_{\xi\xi\xi} - D_2\Theta\right)_\xi = 0 \text{, in } Q \tag{10}$$

where $\lambda_A = \varepsilon^{-1} H/\sqrt{3}$, $\lambda_B = \varepsilon^{-1} g$, $D_1 = \dfrac{a(3\lambda+2\mu)}{\rho c_e}$, $D_2 = \dfrac{T_o a(3\lambda+2\mu)}{\rho c_p^2}$,

The convection boundary condition in nondimensional form is

$$\Theta_\xi = \mathrm{Bi}\left(\Theta - \Theta_\infty\right) \text{ , on } \xi = 0,\ \eta \in (0, J)\,, \tag{11}$$

where $\mathrm{Bi} = \varepsilon C_c / k$ is the nondimensional Biot number characterizing the magnitude of convective heat transfer with respect to that of heat conduction. Note that for $\mathrm{Bi} \to \infty$ the free surface of the half space attains the temperature Θ_∞ and the Robin condition (11) becomes $\Theta(\xi = 0, \eta) = \Theta_\infty(\eta)$. Zero traction conditions at the free surface of the half-space and conditions at infinity now read

$$U_{\xi\xi} = 0 \quad \text{and} \quad \lambda_A^2 U_{\xi\eta\eta} + U_\xi - \lambda_B^2 U_{\xi\xi\xi} - D_2\Theta = 0 \text{, on } \xi = 0,\ \ \eta \in (0, J) \tag{12}$$

$$\lim_{\xi\to\infty} \Theta, U, U_\xi = 0,\ \eta \in (0, J)\,. \tag{13}$$

Finally, the initial conditions (7) become

$$\Theta(\xi, 0) = U(\xi, 0) = U_\eta(\xi, 0) = 0 \text{ for all } \xi \in (0, \infty)\,. \tag{14}$$

The above introduced nondimensional quantities are the ones typically used for the analysis of homogeneous materials in order to introduce a space-time frame suitable for studying the transient effects of thermal shock problems [27, 28, 31]. Notice that in the case of the classical elastic half space subjected to thermal shock, no other characteristic length than ε is introduced.

Setting $D_1 = 0$, results in the elimination of the coupling term $U_{\xi\eta}$ from the heat transfer equation (9). The corresponding weakly coupled system gives rise to the problem of thermal stresses in a gradient elastic half space.

4. Variational Formulation

In this section, the variational formulation of the previously stated IBVP will be derived. Let us first introduce some notation regarding the appropriate function spaces for the solution of the weak form. The standard notation $H^k(\Omega)$, $k \in \mathbb{N}$ is used for the Hilbert (Sobolev) function spaces $W^{k,2}(\Omega)$ over the open domain Ω and $H^0(\Omega) \equiv L^2(\Omega)$. For $J \in \mathbb{R}_+$ and every Banach space V the function valued space $L^2(0, J; V)$, equipped with the norm

$$\|v\|_{L^2(0,J;V)} \doteq \left(\int_0^J \|v\|_V^2 \, d\eta \right)^{1/2}.$$

will be extensively used (see for example [40]).

Multiply equations (9), (10) with $\vartheta \in H^1(0,\infty)$, $v \in H^2(0,\infty)$, respectively. Assuming enough regularity, integration by parts and use of boundary conditions (11) and (12) along with conditions at infinity, yields the variational problem:

Find Θ, U such that

$$\int_0^\infty \vartheta \Theta_\eta d\xi + \int_0^\infty \vartheta_\xi \Theta_\xi d\xi + \mathrm{Bi}\,\vartheta(0)\Theta(0,\eta) + D_1 \int_0^\infty \vartheta U_{\xi\eta} d\xi = \mathrm{Bi}\,\vartheta(0)\Phi f(\eta\varepsilon / c_p), \quad (15)$$

a.e. in $(0, J)$, for every $\vartheta \in H^1(0,\infty)$ and

$$\int_0^\infty v U_{\eta\eta} d\xi + \lambda_A^2 \int_0^\infty v_\xi U_{\xi\eta\eta} d\xi + \int_0^\infty v_\xi U_\xi d\xi + \lambda_B^2 \int_0^\infty v_{\xi\xi} U_{\xi\xi} d\xi - D_2 \int_0^\infty v_\xi \Theta d\xi = 0, \quad (16)$$

a.e. in $(0, J)$, for every $v \in H^2(0,\infty)$, along with the corresponding homogeneous initial conditions.

In the following stability estimates for the weak solution of the above variational problem will be derived. We will first consider the uncoupled (or weakly coupled) case since in many applications the difference in the response of the fully coupled and weakly coupled systems is negligible [29, 31].

5. The weakly coupled system

In the case where $D_1 = 0$, the thermoelastic system (9), (10) becomes uncoupled, since equation (9) for the temperature field does not depend upon the displacement. In this case, the initial boundary value problem becomes

$$\int_0^\infty v U_{\eta\eta} d\xi + \lambda_A^2 \int_0^\infty v_\xi U_{\xi\eta\eta} d\xi + \int_0^\infty v_\xi U_\xi d\xi + \lambda_B^2 \int_0^\infty v_{\xi\xi} U_{\xi\xi} d\xi = D_2 \int_0^\infty v_\xi F d\xi \ , \quad (17)$$

a.e. in $(0, J)$, for every $v \in H^2(0,\infty)$,

where F is the temperature profile inside the half-space, given as the solution of initial-boundary value problem

$$\Theta_\eta - \Theta_{\xi\xi} = 0, \text{ in } Q. \quad (18)$$

with the convection boundary condition (11), $\lim_{\xi\to\infty} \Theta(\xi,\eta) = 0$ and initial condition $\Theta(\xi, \eta = 0) = 0$.

In the following an energy balance equation will be derived and energy type stability estimates will be proved. Setting $v = U_\eta$ in (17), and using the identities

$$\int_0^\infty U_\eta U_{\eta\eta} d\xi = \frac{1}{2}\frac{d}{d\eta}\left\|U_\eta\right\|^2_{L^2(0,\infty)}\ ,\ \int_0^\infty U_{\xi\eta} U_{\xi\eta\eta} d\xi = \frac{1}{2}\frac{d}{d\eta}\left|U_\eta\right|^2_{H^1(0,\infty)} \quad \text{and}$$

$$\int_0^\infty U_{\xi\eta} U_\xi d\xi + \lambda_B^2 \int_0^\infty U_{\xi\xi\eta} U_{\xi\xi} d\xi = \frac{1}{2}\frac{d}{d\eta}\left[\left|U\right|^2_{H^1(0,\infty)} + \lambda_B^2 \left|U\right|^2_{H^2(0,\infty)}\right],$$

we get for $s = \eta$

$$\frac{d}{ds}\left\|U_s\right\|^2_{L^2(0,\infty)} + \lambda_A^2 \frac{d}{ds}\left|U_s\right|^2_{H^1(0,\infty)} + \frac{d}{ds}\left[\left|U\right|^2_{H^1(0,\infty)} + \lambda_B^2 \left|U\right|^2_{H^2(0,\infty)}\right] = 2D_2 \int_0^\infty U_{\xi s} F d\xi\,, \quad (19)$$

where $\left|\bullet\right|_{H^k(0,\infty)}$ is the standard seminorm in $H^k(0,\infty)$.

Integrating equation (19) with respect to the temporal variable from $s = 0$ to $s = \eta \le J$, and setting

$$E(\eta;\lambda_A,\lambda_B) = \left\|U_\eta\right\|^2_{L^2(0,\infty)} + \lambda_A^2 \left|U_\eta\right|^2_{H^1(0,\infty)} + \left|U\right|^2_{H^1(0,\infty)} + \lambda_B^2 \left|U\right|^2_{H^2(0,\infty)}, \quad (20)$$

$$P(\eta) = D_2 \int_0^\eta \int_0^\infty U_{\xi s} F d\xi ds\ , \quad (21)$$

$$\text{we get } E(\eta;\lambda_A,\lambda_B) = 2P(\eta)\,,\ \forall \eta \in (0, J]\,. \quad (22)$$

Equation (22) expresses an energy balance and will be used in the following as means to verify the quality of the numerical solutions for the problem of thermal stresses inside the gradient elastic half-space. A typical stability estimate of the form

$$\left\|U_\eta\right\|_{L^2(0,J;H^1(0,\infty))} + \left\|U\right\|_{L^2(0,J;H^2(0,\infty))} \le \sqrt{2CJe^{CJ}}\, D_2 \left\|F\right\|_{L^2(0,J;L^2(0,\infty))}, \quad (23)$$

with $C = C(\lambda_A^2, \lambda_B^2) = 1/\min\left[1, \lambda_A^2, \lambda_B^2\right]$ can be shown for the weakly coupled IBVP, in a straightforward manner. Observe that by adding $\int_0^\infty U_\eta U d\xi$ to both sides of (17) it is

$$\begin{aligned}\frac{d}{ds}\left\|U_s\right\|^2_{L^2(0,\infty)} + \lambda_A^2 \frac{d}{ds}\left|U_s\right|^2_{H^1(0,\infty)} + \frac{d}{ds}\left[\left\|U\right\|^2_{L^2(0,\infty)} + \left|U\right|^2_{H^1(0,\infty)} + \lambda_B^2 \left|U\right|^2_{H^2(0,\infty)}\right] \\ = 2D_2 \int_0^\infty U_{\xi s} F d\xi + 2\int_0^\infty U_s U d\xi\end{aligned}\ . \quad (24)$$

Integration with respect to the temporal variable (which is now set to be s) from $s = 0$ to $s = \eta \le \tau$, yields

$$\left\|U_\eta\right\|^2_{L^2(0,\infty)}+\lambda_A^2\left|U_\eta\right|^2_{H^1(0,\infty)}+\left\|U\right\|^2_{L^2(0,\infty)}+\left|U\right|^2_{H^1(0,\infty)}+\lambda_B^2\left|U\right|^2_{H^2(0,\infty)}= 2D_2\int_0^\eta\int_0^\infty U_{\xi s}Fd\xi ds+2\int_0^\eta\int_0^\infty U_s Ud\xi ds \quad . \tag{25}$$

Using Cauchy-Schwarz inequality for the integrals at the r.h.s. of (25) leads to

$$\left\|U_\eta\right\|^2_{L^2(0,\infty)}+\left|U_\eta\right|^2_{H^1(0,\infty)}+\left\|U\right\|^2_{L^2(0,\infty)}+\left|U\right|^2_{H^1(0,\infty)}+\left|U\right|^2_{H^2(0,\infty)}\le 2D_2C\int_0^\eta\left|U_s\right|_{H^1(0,\infty)}\left\|F\right\|_{L^2(0,\infty)}ds+2C\int_0^\eta\left\|U_s\right\|_{L^2(0,\infty)}\left\|U\right\|_{L^2(0,\infty)}ds \quad , \tag{26}$$

where $C=C(\lambda_A^2,\lambda_B^2)=1/\min\left[1,\lambda_A^2,\lambda_B^2\right]$. Using inequality $2\alpha\beta\le\alpha^2+\beta^2$ for real positive numbers we get

$$\left\|U_\eta\right\|^2_{H^1(0,\infty)}+\left\|U\right\|^2_{H^2(0,\infty)}\le C\int_0^\eta\left(\left|U_s\right|^2_{H^1(0,\infty)}+D_2^2\left\|F\right\|^2_{L^2(0,\infty)}\right)ds+C\int_0^\eta\left(\left\|U_s\right\|^2_{L^2(0,\infty)}+\left\|U\right\|^2_{L^2(0,\infty)}\right)ds \quad . \tag{27}$$

and applying Gronwall's lemma

$$\left\|U_\eta\right\|^2_{H^1(0,\infty)}+\left\|U\right\|^2_{H^2(0,\infty)}\le D_2^2Ce^{CJ}\left\|F\right\|^2_{L^2(0,J;L^2(0,\infty))} \quad . \tag{28}$$

Integrating with respect to time in $(0,J)$

$$\left\|U_\eta\right\|^2_{L^2(0,J;H^1(0,\infty))}+\left\|U\right\|^2_{L^2(0,J;H^2(0,\infty))}\le D_2^2CJe^{CJ}\left\|F\right\|^2_{L^2(0,J;L^2(0,\infty))}. \tag{29}$$

Taking square roots and using norm equivalence in $\mathbb{R}^2$, yields

$$\left\|U_\eta\right\|_{L^2(0,J;H^1(0,\infty))}+\left\|U\right\|_{L^2(0,J;H^2(0,\infty))}\le c\left\|F\right\|_{L^2(0,J;L^2(0,\infty))}\ ,\ c=D_2\sqrt{2CJe^{CJ}}\ . \tag{30}$$

If $\lambda_A,\lambda_B\ge 1$, it is $C=1$ and $c\sim e^{J/2}$. However, if $\lambda_A<1$ or $\lambda_B<1$, notice that $c\sim\lambda_{A,B}^{-1}e^{(\lambda_{A,B}^2)J/2}$. Typically it is $\lambda_{A,B}^{-2}\gg 1$ and the exponential growth of the constant c becomes extremely rapid. A somewhat more elaborate analysis yields an improved constant for the desired stability estimate. In particular, working in the same spirit as in [41], great care has been exercised in order to avoid any exponential dependence of the stability constants upon quantities of the form λ_A^{-1} or λ_B^{-1} or the Biot number Bi when $\lambda_A,\lambda_B<1$ or in cases where $\mathrm{Bi}>1$. In the following, a stability result with a constant that exhibits only linear growth with $\lambda_A^{-1}\gg 1$ will be derived. For that purpose the first step is to slightly modify the norms used for the stability estimate and then make use

Young's inequality in the form $2\alpha\beta \le \varepsilon\alpha^2 + \varepsilon^{-1}\beta^2$, $\varepsilon \in \mathbb{R}_+$, for real positive numbers α, β, selecting appropriately the value for ε. We begin with the following definition:

Definition For any set of real positive numbers λ_k, $k \in \mathbb{N}$ we introduce the spaces $\Upsilon_k \equiv H^k(0,\infty)$, $k = 1,2,3,...$ and $\Upsilon_0 \equiv L^2(0,\infty)$, equipped with the norm

$$\|u\|_{\Upsilon_k}^2 \doteq \|u\|_{H^{k-1}(0,\infty)}^2 + \lambda_k^2 |u|_{H^k(0,\infty)}^2,\ \lambda_k \in \mathbb{R}_+. \tag{31}$$

It can be easily verified that the norms defined in eq. (31), are equivalent to the standard norms in $H^k(\Omega)$ i.e. $c_k \|u\|_{H^k(0,\infty)} \le \|u\|_{\Upsilon_k} \le C_k \|u\|_{H^k(0,\infty)}$, $k \in \mathbb{N}$ and $c_k = \min[1, \lambda_k]$ and $C_k = \max[1, \lambda_k]$.

Finally, it is by definition $E(\eta; \lambda_A, \lambda_B) = \|U_\eta\|_{\Upsilon_1}^2 + \|U\|_{\Upsilon_2}^2 - \|U\|_{L^2(0,\infty)}^2$. We may now prove the following

THEOREM 1 *Let $\lambda_A \in (0,1)$ and assume that the solution of variational problem (15), (16) with $D_1 = 0$ is sufficiently regular. Then it is*

$$\|U_\eta\|_{L^2(0,J;\Upsilon_1)} + \|U\|_{L^2(0,J;\Upsilon_2)} \le \lambda_A^{-1} D_2 \sqrt{2Je^J}\, \|F\|_{L^2(0,J;L^2(0,\infty))}, \tag{32}$$

Proof Using the same steps as previously, one easily gets

$$\begin{aligned} &\|U_\eta\|_{L^2(0,\infty)}^2 + \lambda_A^2 |U_\eta|_{H^1(0,\infty)}^2 + \|U\|_{L^2(0,\infty)}^2 + |U|_{H^1(0,\infty)}^2 + \lambda_B^2 |U|_{H^2(0,\infty)}^2 \le \\ &\qquad 2D_2 \int_0^\eta |U_s|_{H^1(0,\infty)} \|F\|_{L^2(0,\infty)}\, ds + 2\int_0^\eta \|U_s\|_{L^2(0,\infty)} \|U\|_{L^2(0,\infty)}\, ds \end{aligned}. \tag{33}$$

From this point on, the analysis follows a different path. Invoking the definition of the Υ_k, $k = 1,2$ norms in order to group the terms in the l.h.s. of (33) and using Young's inequality, with $\varepsilon = \lambda_A^2$, it is

$$\|U_\eta\|_{\Upsilon_1}^2 + \|U\|_{\Upsilon_2}^2 \le \int_0^\eta \left(\lambda_A^2 |U_s|_{H^1(0,\infty)}^2 + \lambda_A^{-2} D_2^2 \|F\|_{L^2(0,\infty)}^2 + \|U_s\|_{L^2(0,\infty)}^2 + \|U\|_{L^2(0,\infty)}^2 \right) ds \ . \tag{34}$$

For the r.h.s. of (34), we may write

$$\begin{aligned} &\int_0^\eta \left(\lambda_A^2 |U_s|_{H^1(0,\infty)}^2 + \lambda_A^{-2} D_2^2 \|F\|_{L^2(0,\infty)}^2 + \|U_s\|_{L^2(0,\infty)}^2 + \|U\|_{L^2(0,\infty)}^2 \right) ds \le \\ &\qquad \int_0^\eta \left(\|U_s\|_{\Upsilon_1}^2 + \|U\|_{\Upsilon_2}^2 \right) ds + \lambda_A^{-2} D_2^2 \int_0^\eta \|F\|_{L^2(0,\infty)}^2\, ds \end{aligned}, \tag{35}$$

Application of Gronwall's lemma yields

$$\left\|U_\eta\right\|^2_{\Upsilon_1} + \left\|U\right\|^2_{\Upsilon_2} \le \lambda_A^{-2} e^\eta D_2^2 \int_0^\eta \left\|F\right\|^2_{L^2(0,\infty)} ds \le \lambda_A^{-2} e^J D_2^2 \left\|F\right\|^2_{L^2(0,J;(0,\infty))} , \quad (36)$$

Integrating again with respect to η

$$\left\|U_\eta\right\|^2_{L^2(0,J;\Upsilon_1)} + \left\|U\right\|^2_{L^2(0,J;\Upsilon_2)} \le \lambda_A^{-2} J e^J D_2^2 \left\|F\right\|^2_{L^2(0,J;L^2(0,\infty))} . \quad (37)$$

Taking now square roots and using the norm equivalence in $\mathbb{R}^2$, we arrive at (32). □

REMARK. Observe that in this case it is $c \sim \lambda_A^{-1} e^{J/2}$ and the dependence of the stability constant on the large term λ_A^{-1} is only linear and not exponential. Furthermore, note that in this case the stability constant does not depend on λ_B. Finally, let us mention, that an analogous procedure may be used to derive energy norm error estimates for the finite element method. The derivation of these estimates will be the subject of a future work.

6. The fully coupled system

In this section, an *a priori* stability result for the weak solution of the fully coupled thermoelastic problem will be derived. The estimate presented here is sharper than that obtained in [42].

THEOREM 2 *Let* $\omega = D_2 / D_1 > 0$ and *assume that the solution of variational problem (15), (16) is sufficiently regular. Then it is*

$$\left\|U_s\right\|_{L^2(0,J;\Upsilon_1)} + \left\|U\right\|_{L^2(0,J;\Upsilon_2)} + \left\|\Theta\right\|_{L^2(0,J;L^2_\omega(0,\infty))} \le \mathrm{Bi}\Phi J \sqrt{3\omega e^J}\, \left\|\delta\right\|_{H^1(0,\infty)^*} . \quad (38)$$

Proof Set $\vartheta = \Theta$ in (15) and $v = U_\eta$ in (16). Multiply equation (15) by ω, add (15) to (16) and note the resulting mutual cancelation of the coupling terms

$$D_1 \int_0^\infty \vartheta U_{\xi\eta} d\xi \text{ and } -D_2 \int_0^\infty v_\xi \Theta d\xi . \quad (39)$$

The variational equation now reads

$$\begin{aligned} &\int_0^\infty U_\eta U_{\eta\eta} d\xi + \lambda_A^2 \int_0^\infty U_{\xi\eta} U_{\xi\eta\eta} d\xi + \int_0^\infty U_{\xi\eta} U_\xi d\xi + \lambda_B^2 \int_0^\infty U_{\xi\xi\eta} U_{\xi\xi} d\xi \\ &\quad + \omega \int_0^\infty \Theta\Theta_\eta d\xi + \omega \int_0^\infty \Theta_\xi \Theta_\xi d\xi + \mathrm{Bi}\omega\Theta(0,\eta)^2 = \mathrm{Bi}\omega\Phi\, f(\eta\varepsilon / c_p) \left\langle \Theta, \delta(\xi) \right\rangle \end{aligned} , \quad (40)$$

where $\left\langle \cdot,\cdot \right\rangle$ denotes the pairing between $H^1(0,\infty)$ and its dual space $H^1(0,\infty)^*$. In fact, as will be shown later, the Dirac function $\delta(\xi)$ is smoother than required for the duality

pairing to make sense in this 1D setting. Adding the term $\int_0^\infty U_\eta U d\xi$ to both sides of eq. (40), we may write, since $|f| \le 1$,

$$\begin{aligned} &\frac{d}{ds}\|U_s\|^2_{L^2(0,\infty)} + \lambda_A^2 \frac{d}{ds}|U_s|^2_{H^1(0,\infty)} + \frac{d}{ds}\left[\|U\|^2_{L^2(0,\infty)} + |U|^2_{H^1(0,\infty)} + \lambda_B^2 |U|^2_{H^2(0,\infty)}\right] \\ &+ \frac{d}{ds}\|\Theta\|^2_{L^2_\omega(0,\infty)} \le |2\mathrm{Bi}\omega\Phi f(\eta)|\left|\langle\Theta, \delta(\xi)\rangle\right| - \omega|\Theta|^2_{H^1(0,\infty)} + 2\int_0^\infty U_s U d\xi \le \\ &|2\mathrm{Bi}\omega\Phi|\left|\langle\Theta, \delta(\xi)\rangle\right| - \omega|\Theta|^2_{H^1(0,\infty)} + 2\int_0^\infty U_s U d\xi \end{aligned} \quad , \quad (41)$$

where $\|u\|_{L^2_\omega(\Omega)} \doteq (\omega u, u)_{L^2(\Omega)}$ denotes the ω - weighted L^2 inner product.

Using Cauchy-Schwarz inequality for the duality pairing, the definitions of the norms in spaces Υ_1 and Υ_2 and modified Young's inequality with $\varepsilon = 1$ for the second integral in the r.h.s. of (41) we arrive at

$$\begin{aligned} &\frac{d}{ds}\left[\|U_s\|^2_{\Upsilon_1} + \|U\|^2_{\Upsilon_2} + \|\Theta\|^2_{L^2_\omega(0,\infty)}\right] \le \\ &|2\mathrm{Bi}\omega\Phi|\|\Theta\|_{H^1(0,\infty)}\|\delta\|_{H^1(0,\infty)^*} - \omega|\Theta|^2_{H^1(0,\infty)} + \|U_s\|^2_{\Upsilon_1} + \|U\|^2_{\Upsilon_2} \end{aligned} \quad , \quad (42)$$

Employing again the modified Young's inequality with $\varepsilon = |\mathrm{Bi}\Phi|$ and since by definition it is $\|\Theta\|^2_{H^1(0,\infty)} = \|\Theta\|^2_{L^2(0,\infty)} + |\Theta|^2_{H^1(0,\infty)}$, we have

$$\omega\mathrm{Bi}^2\Phi^2\|\delta\|^2_{H^1(0,\infty)^*} + \omega\|\Theta\|^2_{H^1(0,\infty)} - \omega|\Theta|^2_{H^1(0,\infty)} \le \omega\mathrm{Bi}^2\Phi^2\|\delta\|^2_{H^1(0,\infty)^*} + \|\Theta\|^2_{L^2_\omega(0,\infty)} . \quad (43)$$

Using this last inequality in conjunction with (41), integrating with respect to time from $s = 0$ to $s = \eta$ and applying Gronwall's lemma, we finally arrive at

$$\|U_\eta\|^2_{\Upsilon_1} + \|U\|^2_{\Upsilon_2} + \|\Theta\|^2_{L^2_\omega(0,\infty)} \le \omega\mathrm{Bi}^2\Phi^2 J\|\delta\|^2_{H^1(0,\infty)^*} e^J , \quad (44)$$

Integrating again with respect to time from $\eta = 0$ to $\eta = J$, taking square roots and using the norm equivalence in $\mathbb{R}^3$ we get estimate (38). □

7. Semi-discretization with Finite Elements and time integration

Let us now introduce appropriate finite element spaces for conforming discretization of the variational problem (15), (16). A first step is the approximation of the infinite domain $(0,\infty)$ with a finite one $(0, L(J))$, where the end point is selected such that conditions at infinity hold approximately in $L(J) \in \mathbb{R}_+$ for $\eta < J$. A similar procedure has been adopted in [43] for the solution of a Cauchy problem of nonlinear, classical

thermoelasticity. For the approximation of the temperature field we select $V_\Theta^h \subset H^1(0,L)$, such that for each fixed $\bar{\eta} \in (0, J]$, it is $\Theta^h(\bar{\eta}) \in V_\Theta^h$, where h is the characteristic mesh size. Similarly, for the approximation of the displacement field we have $U^h(\bar{\eta}) \in V_U^h \subset H^2(0,L)$. The discretized variational problem becomes

Find Θ^h, U^h such that

$$\begin{aligned} \int_0^L \vartheta^h \Theta_\eta^h d\xi + \int_0^L \vartheta_\xi^h \Theta_\xi^h d\xi + \mathrm{Bi}\, \vartheta^h(0)\Theta^h(0,\eta) \\ + D_1 \int_0^L \vartheta^h U_{\xi\eta}^h d\xi = \vartheta^h(0)\mathrm{Bi}\Phi f(\eta\varepsilon / c_p) \end{aligned}, \tag{45}$$

a.e. in $(0, J)$ for every $\vartheta^h \in V_\Theta^h$ and

$$\begin{aligned} \int_0^L v^h U_{\eta\eta}^h d\xi + \lambda_A^2 \int_0^L v_\xi^h U_{\xi\eta\eta}^h d\xi + \int_0^L v_\xi^h U_\xi^h d\xi \\ + \lambda_B^2 \int_0^L v_{\xi\xi}^h U_{\xi\xi}^h d\xi - D_2 \int_0^L v_\xi^h \Theta^h d\xi = 0 \end{aligned}, \tag{46}$$

a.e. in $(0, J)$ for every $v^h \in V_U^h$.

The selected finite element approximations feature 5th order Hermite polynomials for the approximation of the displacement field and quadratic Lagrange shape functions for the approximation of the temperature. The respective finite element spaces are defined, for $\bar{\eta} \in (0, J)$ random but fixed, as

$$V_\Theta^h = \left\{ w^h \in H^1(0,L) : w^h\big|_e = \sum_{i=1}^{3} L_i(x) w_i^h(\bar{\eta}) \right\}, \text{ and} \tag{47}$$

$$V_U^h = \left\{ w^h \in H^2(0,L) : w^h\big|_e = \sum_{i=1}^{6} H_i(x) w_i^h(\bar{\eta}) \right\}. \tag{48}$$

Note that in order to formulate conforming finite element approximations the use of Hermite interpolation polynomials is necessary, as the weak solution for the displacements has been found to be in $H^2(0,\infty)$ for each $\eta \in (0, J)$ and thus higher regularity that that yielded by Lagrange interpolation polynomials is needed.

Finally, it is worth noting that similar combinations of C^0 (temperature field) and C^1 (gradient elastic displacement field) have also been applied other coupled field problems, as for example the simulation of the hydroelastic response of thin flexible strips subjected to long water wave excitation [44].

Discretization in space with finite elements produces a system of Ordinary Differential Equations (ODEs) to be integrated with respect to time. This system has the form

$$\mathbf{M}\mathbf{y}_{\eta\eta} + \mathbf{C}\mathbf{y}_{\eta} + \mathbf{K}\mathbf{y} = \mathbf{F}, \tag{49}$$

where $\mathbf{y}$ is the vector on nodal unknowns $\Theta_i^h, U_i^h, U_{\xi i}^h$, and subscript i ranges over all the mesh nodes. Introducing the vector $\mathbf{v} = \mathbf{y}_{\eta}$ system (49) is transformed to the first order in time system

$$\begin{bmatrix} \mathbf{I} & \mathbf{O} \\ \mathbf{O} & \mathbf{M} \end{bmatrix} \begin{bmatrix} \mathbf{y}_{\eta} \\ \mathbf{v}_{\eta} \end{bmatrix} + \begin{bmatrix} \mathbf{O} & -\mathbf{I} \\ \mathbf{K} & \mathbf{C} \end{bmatrix} \begin{bmatrix} \mathbf{y} \\ \mathbf{v} \end{bmatrix} = \begin{bmatrix} \mathbf{0} \\ \mathbf{F} \end{bmatrix}. \tag{50}$$

For a time step $\tau > 0$, selected such that it is $\tau = J / n$, $n \in \mathbb{N}$, the time integration of system (50) is performed with the general scheme,

$$\mathbf{A}(a)\mathbf{z}_{n+1} + \mathbf{B}(a)\mathbf{z}_n = \mathbf{f}, \tag{51}$$

where, for a parameter $a \in [0,1]$, it is

$\mathbf{A}(a) = \begin{bmatrix} \mathbf{I} & \mathbf{O} \\ \mathbf{O} & \mathbf{M} \end{bmatrix} + a\tau \begin{bmatrix} \mathbf{O} & -\mathbf{I} \\ \mathbf{K} & \mathbf{C} \end{bmatrix}$, $\mathbf{B}(a) = (1-a)\tau \begin{bmatrix} \mathbf{O} & -\mathbf{I} \\ \mathbf{K} & \mathbf{C} \end{bmatrix} - \begin{bmatrix} \mathbf{I} & \mathbf{O} \\ \mathbf{O} & \mathbf{M} \end{bmatrix}$, $\mathbf{z} = \begin{bmatrix} \mathbf{y} \\ \mathbf{v} \end{bmatrix}$ and

$\mathbf{f} = a\tau \begin{bmatrix} \mathbf{0} \\ \mathbf{F}_{n+1} \end{bmatrix} + (1-a)\tau \begin{bmatrix} \mathbf{0} \\ \mathbf{F}_{n+1} \end{bmatrix}$.

The cases $a = 0,1/2,1$ correspond to the Explicit Euler, Crank-Nicolson and Implicit Euler method respectively. The explicit scheme for $a = 0$ is not unconditionally stable and therefore it will not be considered in the following. The Crank-Nicolson scheme is second order accurate and A-stable but not L-stable. Finally, the Implicit Euler method has excellent stability properties but is only first order accurate. In the following analysis, the value $a = 0.52$ has been considered. This value is selected in order to introduce an amount of numerical dissipation to the solution. Note that when $a = 0.5$, the classical elasticity solution exhibits spurious oscillations near sharp fronts when relatively coarse time stepping is employed. A more detailed discussion of this phenomenon will be presented in the following section.

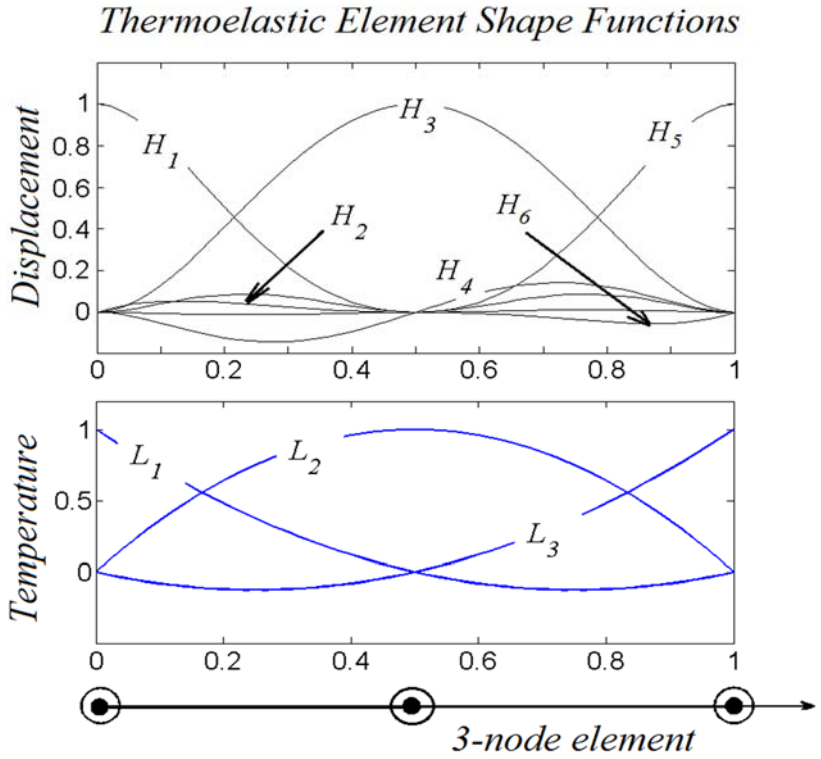

Figure 3. Thermoelastic element shape functions. The element features 5th order Hermite polynomials for the approximation of the displacement field and quadratic Lagrange shape functions for the approximation of the temperature.

8. Results and discussion

The problem of thermal shock response for the gradient elastic half-space is solved for two different values of the Biot Number, $\mathrm{Bi}=1$ and $\mathrm{Bi}=\infty$. The latter value corresponds to the application of a Dirichlet condition on the upper surface of the half space, such that the temperature at this point attains the value Θ_∞ immediately at time $\eta=0$, as also discussed in previous sections. In both cases we set $f=\mathcal{H}(\eta-0)$, where Φ is set to unity in eq. (5). The numerical solution for the displacement field is obtained by discretizing the region, $[0,L]$ where $L=L(J)\in\mathbb{R}_+$ is properly selected so as to avoid any wave reflections at $\xi=L$ in the time interval examined.

In the present study, we examine the effects of the relative magnitude of the (nondimensional) microstructural parameters $\lambda_A=\varepsilon^{-1}H/\sqrt{3}$ and $\lambda_B=\varepsilon^{-1}g$, controlling micro-inertia and strain gradient effects, respectively, on the mechanical behavior of the material under thermal shock conditions. Estimates relating the gradient parameters H and g with the geometrical characteristics of the material microstructure can be found in [4, 18]. In particular, Shodja et al. [18] showed, via an atomistic

approach, that for several metallic materials and different crystalline structures (fcc or bcc), the characteristic lengths range from about 2 Å to 5 Å. Given that for typical metals (e.g. aluminum, copper, lead, titanium, and steel) and some ceramic materials (e.g. silica) the thermoelastic length ε is of the order of 10Å (at 300K) (see e.g. [45]), the values for the nondimensional parameters λ_A and λ_B range from 0.1 to 0.5. The material properties selected are typical for ceramic refractories and in particular are set to: $k = 33W/mK$, $\rho = 4000kg/m^3$, $c_e = 755J/kgK$, $a = 4.6e-6K^{-1}$, $E = 416e9N/m^2$, $\nu = 0.23$.

The solution is obtained for both the fully and weakly coupled systems. Several numerical tests have been performed in order to evaluate the convergence characteristics of the proposed method. A sequence of finite element meshes is considered. The number of finite elements N_{el} employed for the solution is increased as $N_{el} = 100, 200, 400, 800, 1600$. In all cases we select the number of time steps N_t to be twice the number of the elements ($N_t = 2N_{el}$). Finally, a numerical experiment with 2500 elements and 10000 time steps was performed to be used as a highly accurate numerical solution.

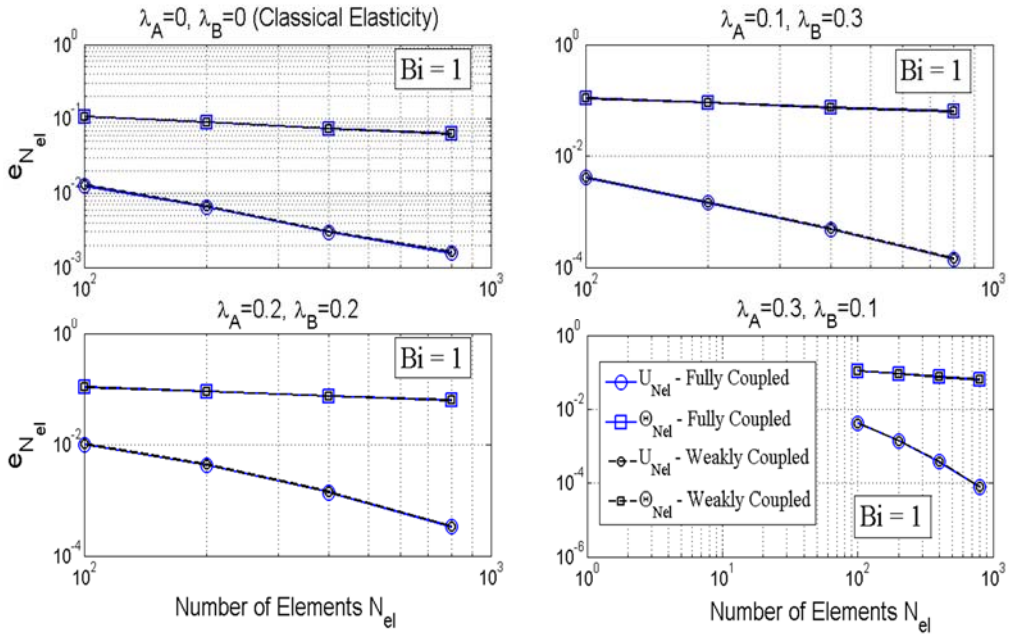

Figure 4. Convergence characteristics of the proposed finite element procedure. Both the temperature and the displacement approximation error are plotted for $\mathrm{Bi} = 1$. Both axes are in logarithmic scale.

An example of the convergence characteristics of the finite element procedure are shown in figure (4) for $\mathrm{Bi} = 1$. Both axes in figure 4 are in logarithmic scale. The

solution obtained with 1600 elements was considered to be the 'exact solution'. As an error indicator, the following quantity has been selected

$$e_{N_{el}} = \frac{\max\limits_{\xi_i \in [0,L], \eta_j \in [0,J]} \left| solution(N_{el} = 1600) - solution(N_{el}) \right|}{\max\limits_{\xi_i \in [0,L], \eta_j \in [0,J]} \left| solution(N_{el} = 1600) \right|} . \tag{52}$$

The maximum difference is calculated over all nodal values of the displacement field and over all discrete time instances. The convergence of the displacement field Finite Element solution is more rapid that of the temperature field. This is attributed to the higher order approximation used for the displacements. Finally, the error values are almost identical for the fully coupled and weakly coupled systems for the considered material parameters. This is due to the small contribution of the coupling term in equation (9).

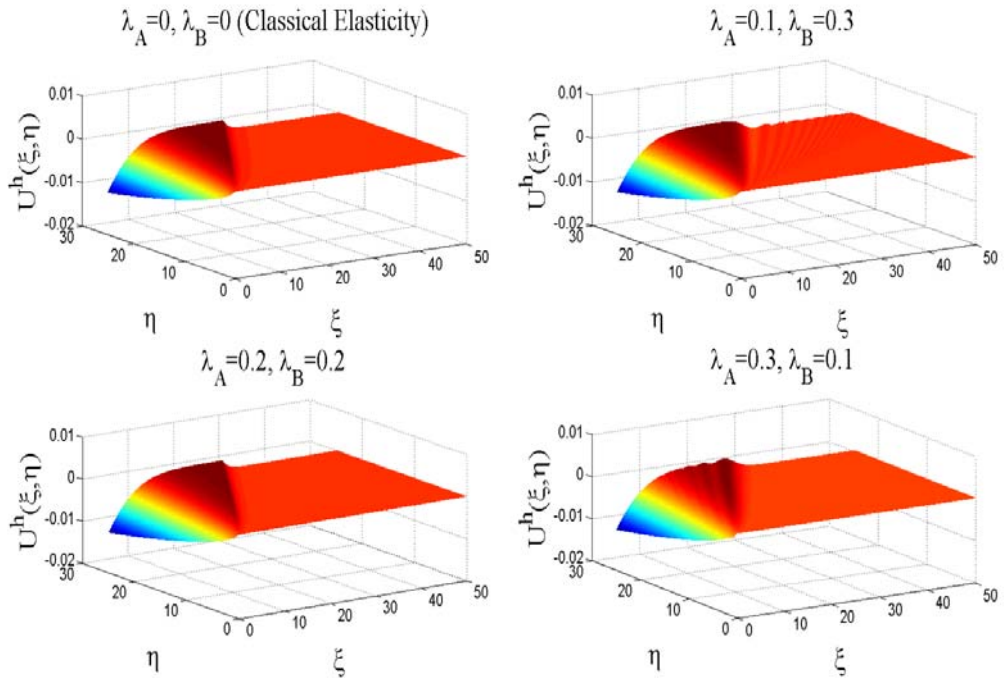

Figure 5. Space - time plot of the displacement field in the fully coupled case inside the gradient elastic half-space for different values of the microstructural parameters λ_A and λ_B and $\mathrm{Bi} = \infty$ Classical elasticity corresponds to the case $\lambda_A = \lambda_B = 0$.

Figure 5 presents a space - time plot of the displacement field inside the gradient elastic half-space for different values of the microstructural parameters λ_A and λ_B (fully coupled system). Classical elasticity corresponds to the case $\lambda_A = \lambda_B = 0$. The results are obtained with 2500 elements and 10000 time steps. The dispersive nature of the

thermoelastic pulse in the case that $\lambda_A = 0.1,\ \lambda_B = 0.3$ and $\lambda_A = 0.3, \lambda_B = 0.1$ can be seen around the pulse traveling front.

Figure 6 illustrates the difference between the solutions of the fully and weakly coupled system. The difference relative to the maximum value attained by the numerical solution of the fully coupled system (denoted in figure 9 as $|||\, U^h_{\text{f/c}}\, |||= \max_{\xi_i \in [0,L], \eta_j \in [0,J]} \left| U^h_{\text{f/c}} \right|$) is plotted. This difference is found to be several orders of magnitude less than the maximum amplitude of the thermoelastic pulse. Thus, the fully coupled and weakly coupled systems yield almost identical results for the considered (ceramic refractory) material.

Let us now study the response of the weakly coupled system. The energy balance for the solution, as dictated by equation (22), is plotted in Figures 6 and 7, for $\mathrm{Bi} = 1$ and $\mathrm{Bi} = \infty$ respectively. In the latter case, the bound dictated by inequality (32), is also computed. Invoking inequality (32) and using the analytical evaluation of the $L^2(0,\eta; L^2(0,\infty))$ norm of the temperature field solution of the heat transfer problem in the half-space cause by a sudden change in the temperature of its boundary, we have

$$\left\| F(\xi, s) \right\|^2_{L^2(0,\eta; L^2(0,\infty))} = \frac{4(2-\sqrt{2})}{3\sqrt{\pi}} \eta^{3/2}, \tag{53}$$

where $F(\xi, s) = \operatorname{erfc}\left(\xi / 2\sqrt{s} \right)$, [28, 29]. In that manner, we obtain an explicit bound for the quantity $E(\eta) \doteq \left\| U_\eta \right\|^2_{\Upsilon_1} + \left\| U \right\|^2_{\Upsilon_2} - \left\| U \right\|^2_{L^2(0,L)}$, where Υ_1, Υ_2 and the induced norms are now defined over the interval $(0, L)$. along with the bound derived from inequality (36) and equation (53). The energy balance for the solution in all cases is verified as $h, \Delta\eta \to 0$, where $\Delta\eta$ denotes the time step.

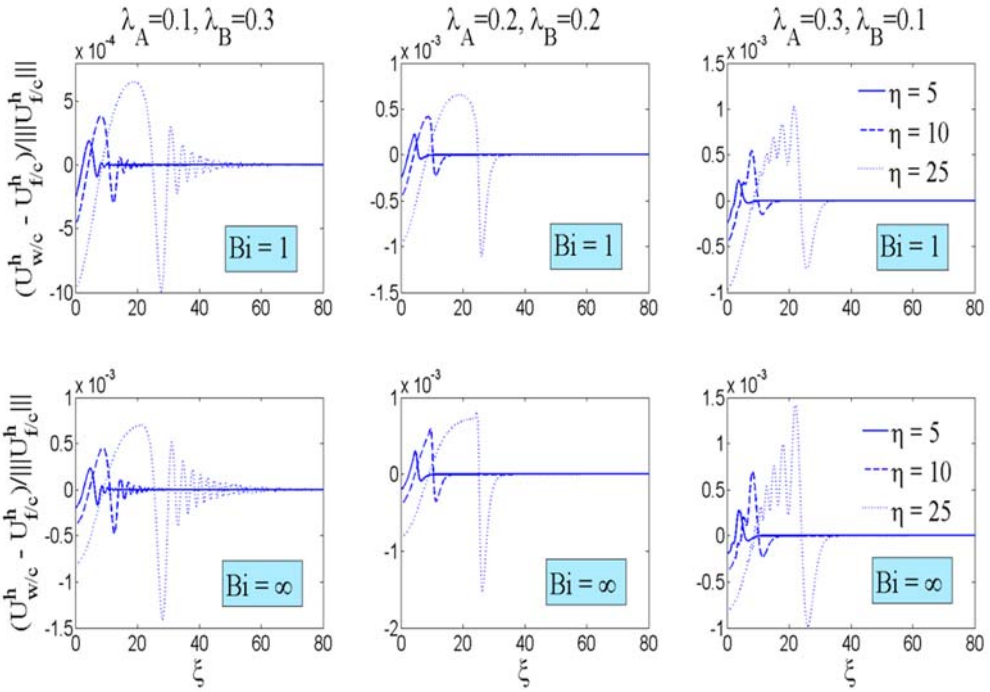

Figure 6. Displacement field solution difference between the fully and weakly coupled systems.

Figures 9 and 10 are plots of the displacement solution for $\mathrm{Bi}=1$ and $\mathrm{Bi}=\infty$ respectively, for the weakly coupled system. In both cases three different combinations of the microstructural parameters are selected. The displacement field is plotted as a function of the spatial parameter at three time instances ($\eta=5,10,25$). The classical elasticity solution ($\lambda_A=\lambda_B=0$) is also plotted. From comparison between Figures 9 and 10 it is observed that the solution is of lower amplitude for small values of the Biot number. The dispersive nature of pulses characterizing gradient elasticity solutions is evident for the cases where the microstructural parameters are dissimilar. Normal dispersion is exhibited in the case where $\lambda_A>\lambda_B$, while anomalous dispersion occurs when $\lambda_A<\lambda_B$. The case ($\lambda_A=\lambda_B=0.2$) shows *almost* zero dispersion. This is in accordance with the dispersion analysis of gradient elastic solutions [32-35, 39].

Figures 11 and 12 are plots of the displacement gradient inside the half-space for $\mathrm{Bi}=1$ and $\mathrm{Bi}=\infty$, respectively. The latter case is of lower regularity for the classical elasticity. However, it is observed that in the case of gradient elasticity, the first derivative of the displacement, corresponding to the strain, is continuous. Note that in the case of the gradient elastic solution, the presence of higher order terms makes the displacement gradient smoother.

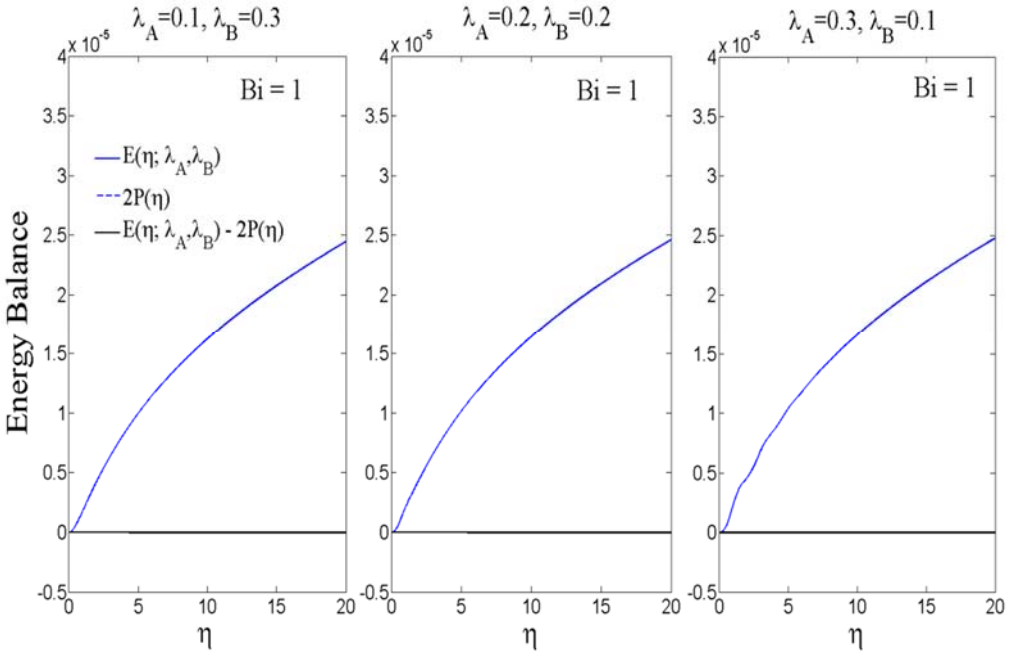

Figure 7. Energy balance according to equation (22), for different values of the microstructural parameters λ_A and λ_B, for $\mathrm{Bi} = 1$.

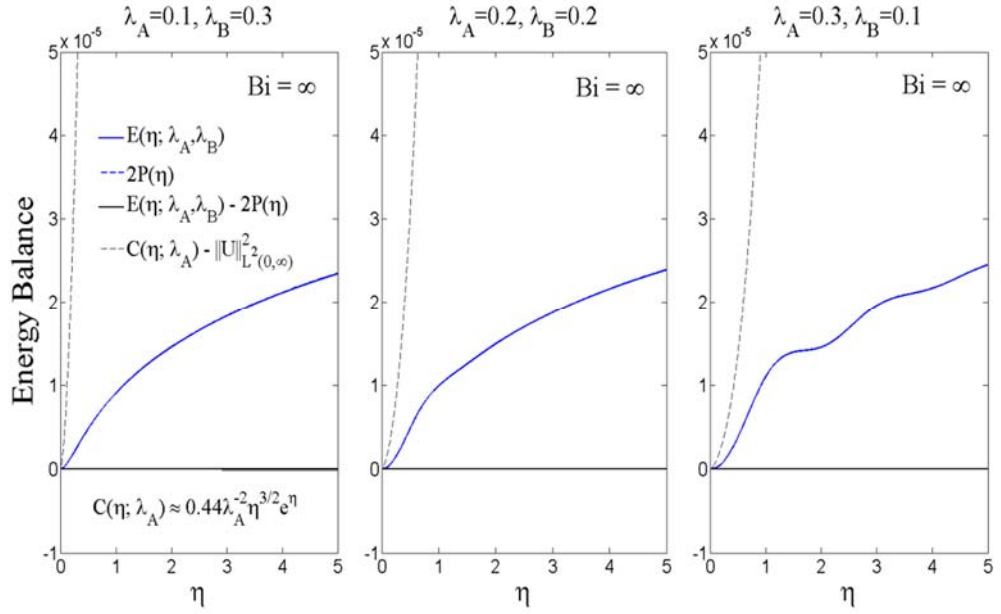

Figure 8. Energy balance according to equation (22), for different values of the microstructural parameters λ_A and λ_B, for $\mathrm{Bi} = \infty$. The stability estimate for the gradient elastic solution (equation (36)) is plotted with a dashed line.

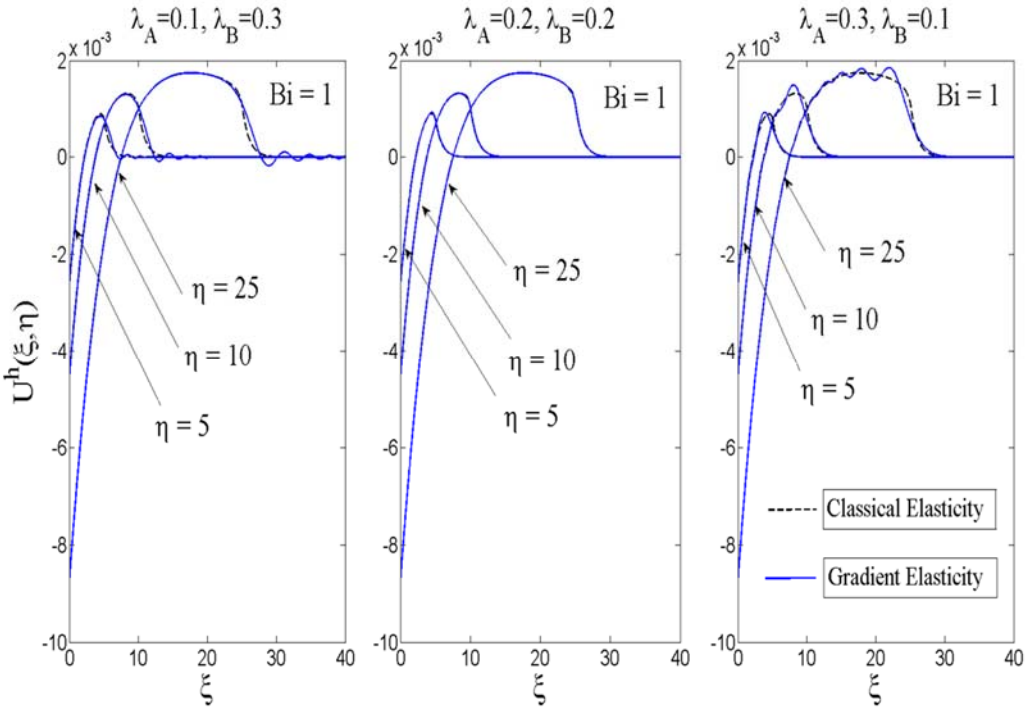

Figure 9. Displacement field inside the half-space for different values of the microstructural parameters λ_A and λ_B, at three time instances. The classical elasticity solution is plotted against the gradient elastic one ($\mathrm{Bi} = 1$).

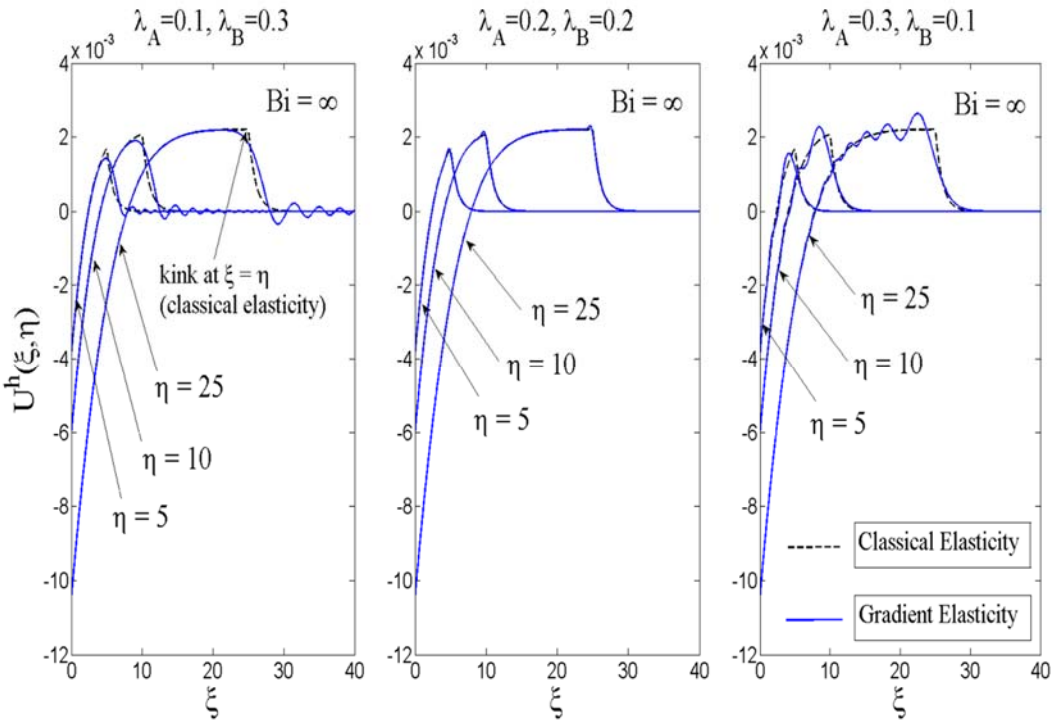

Figure 10. As in Fig. 9 but with $\mathrm{Bi} = \infty$.

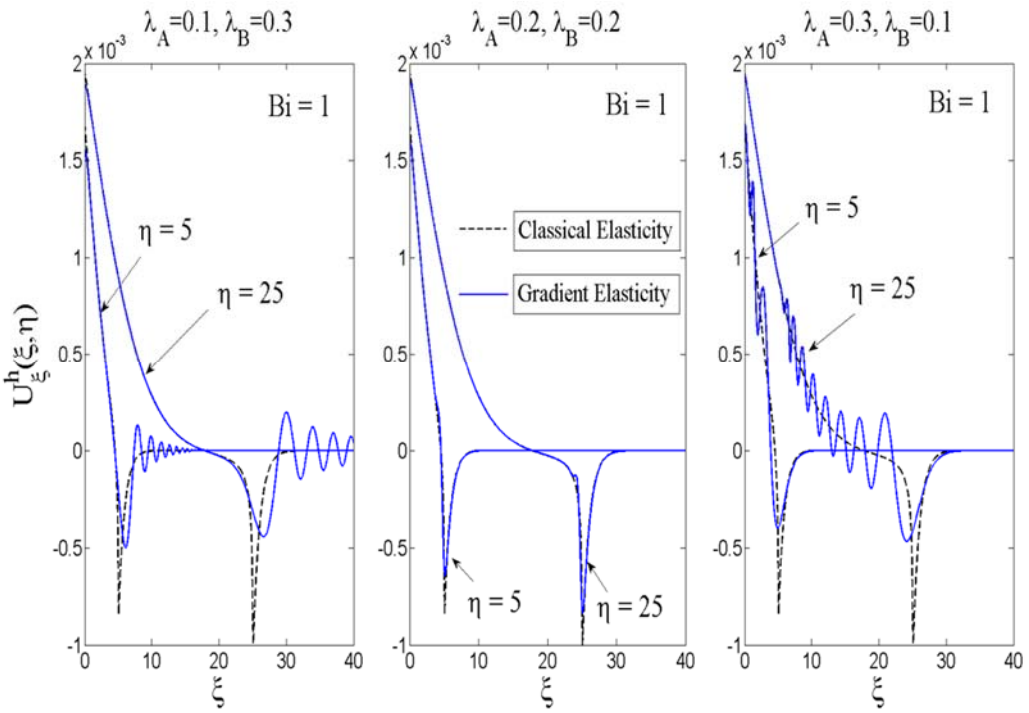

Figure 11. Displacement gradient inside the half-space for different values of the microstructural parameters λ_A and λ_B, at different time instances. The classical elasticity solution is plotted against the gradient elastic one ($\mathrm{Bi} = 1$).

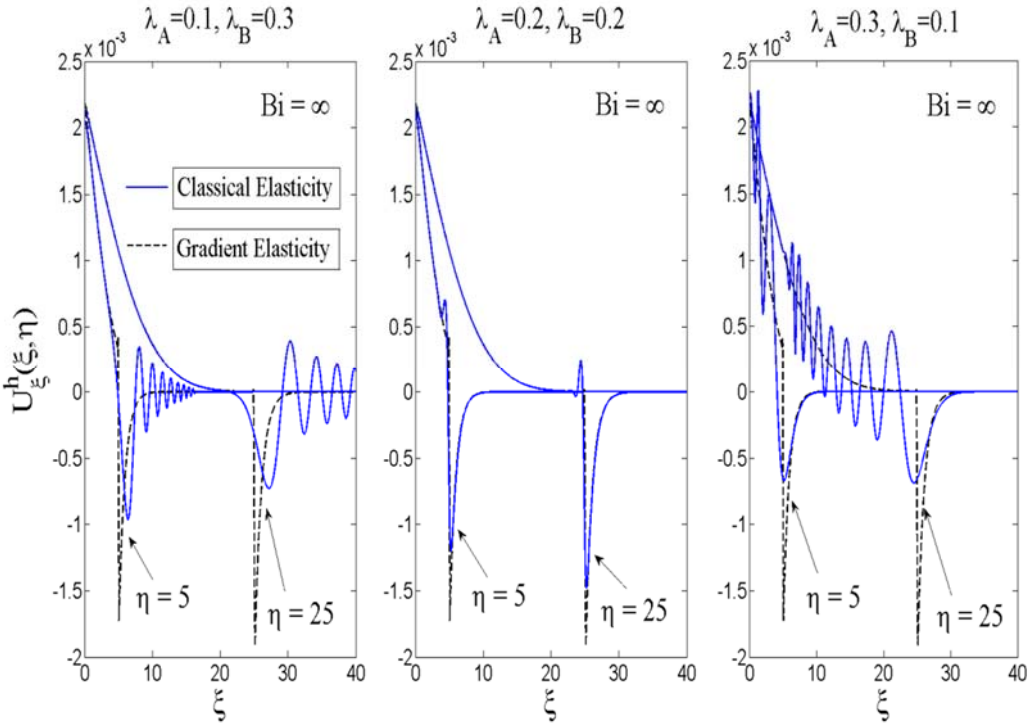

Figure 12. As in Fig. 11 but with $\mathrm{Bi} = \infty$.

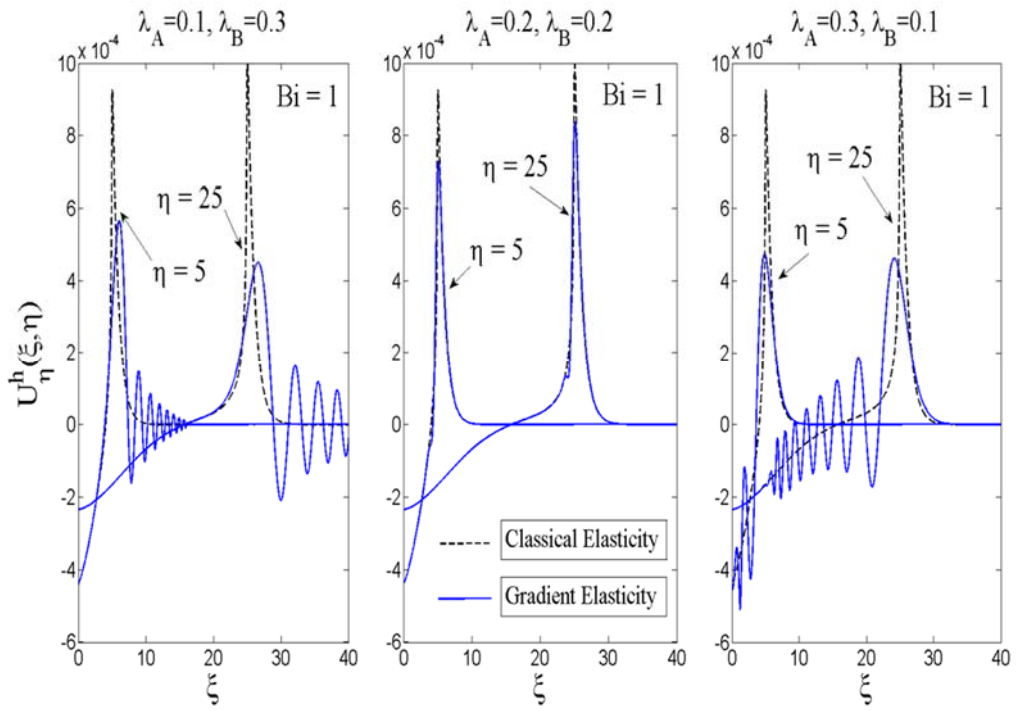

Figure 13. Velocity inside the half-space for different values of the microstructural parameters λ_A and λ_B, at different time instances. The classical elasticity solution is plotted against the gradient elastic one ($\mathrm{Bi} = 1$).

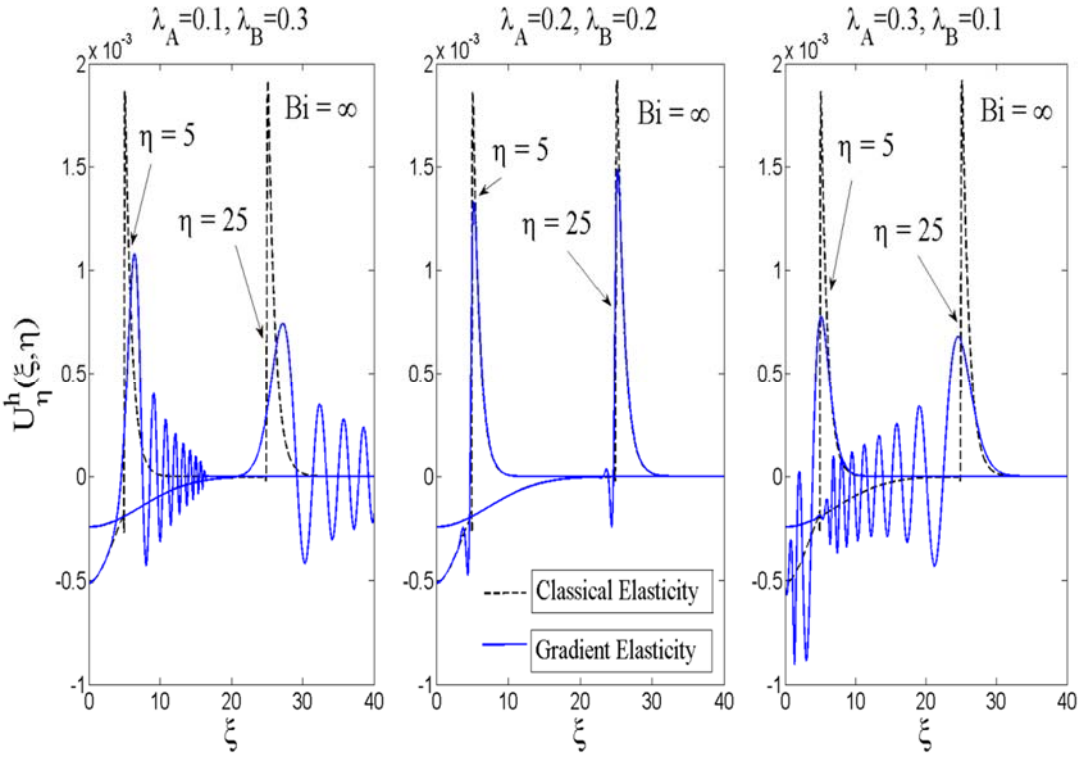

Figure 14. As in Fig. 13 but with $\mathrm{Bi} = \infty$.

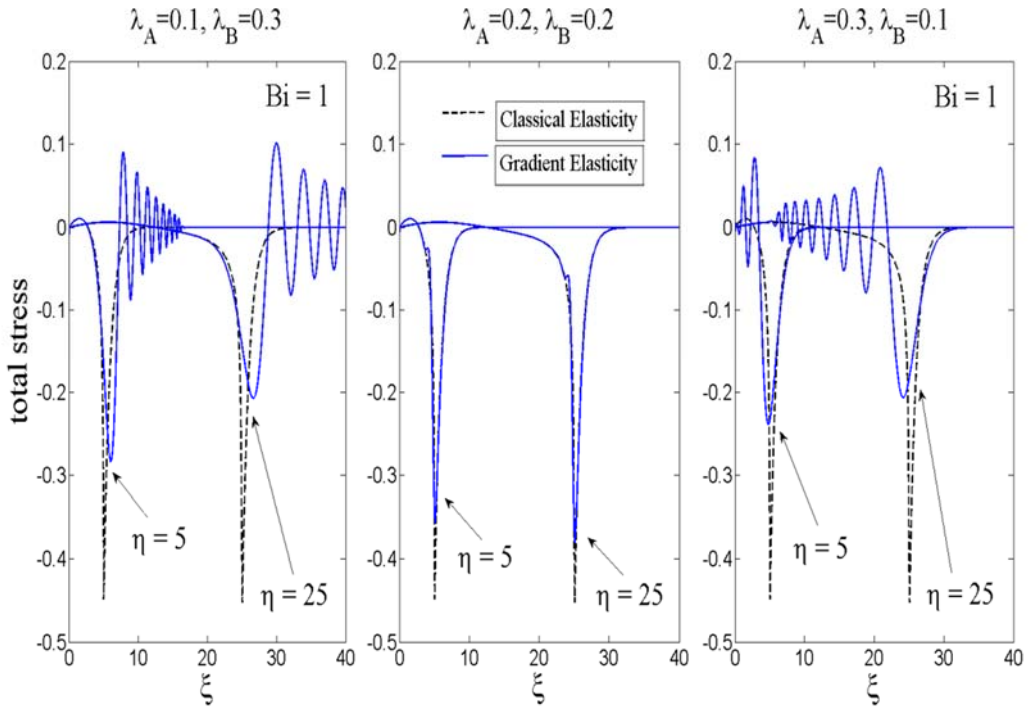

Figure 15. Total stress (eq. (3a)) inside the half-space for different values of the microstructural parameters λ_A and λ_B, at two time instances. The classical elasticity solution is plotted against the gradient elastic one ($\mathrm{Bi} = 1$).

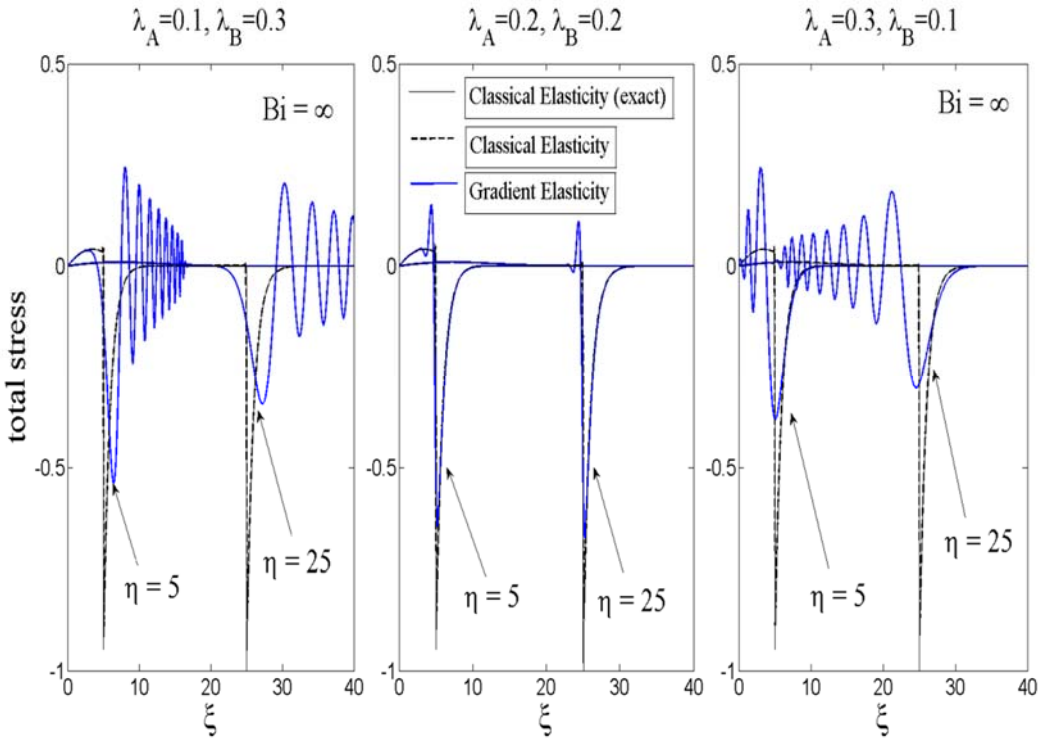

Figure 16. As in Fig. 15 but with $\mathrm{Bi} = \infty$. The exact solution for the stresses [see e.g. 31], is plotted with a thin solid line.

In Figures 13 and 14, the variation of the velocity inside the half-space is displayed for the selected values of the Biot number. Again, three different combinations of the microstructural parameters are selected. The velocity is plotted as a function of the spatial parameter at two time instances ($\eta = 5, 25$). In classical elasticity, for $\mathrm{Bi} = \infty$, the velocity suffers a finite jump at $\eta = \xi$, which implies that a shock wave (singular surface) travels through the material. This is in marked contrast with the gradient elasticity solution where the velocity is continuous and, thus, no shock waves are formed.

Finally, Figures 15 and 16 show the distribution of the (total) stress, defined in Eq. (3a), as a function of the spatial parameter at two time instances ($\eta = 5, 25$) for $\mathrm{Bi} = 1$ and $\mathrm{Bi} = \infty$. Examining the case $\mathrm{Bi} = \infty$ it is observed that in classical elasticity, the monopolar stress (see references [27-31] for a closed form solution of the stress field) exhibits a finite discontinuity at the same point where the velocity becomes discontinuous. The latter observation is a direct consequence of the enforcement of the dynamical compatibility conditions at the singular surface [46]. On the other hand, in the case of gradient elasticity, the total stress remains spatially continuous at all instances. The oscillations appearing before or after the pulse front, at $\eta = \xi$, are the result of the dispersive nature (normal or anomalous) characterizing the gradient elasticity solution.

It is interesting to examine the time profile of the displacement gradient at the free surface of the half space. Figures 17 and 18 depict the displacement gradient for $\xi = 0$ in the case that $\mathrm{Bi} = 1$ and $\mathrm{Bi} = \infty$ respectively. In the former case, namely when $\mathrm{Bi} = 1$ (Figure 17), the strain at the free surface is a continuous function of time. For the classical elasticity, the strain constantly increases (with decreasing rate) approaching asymptotically a certain value. In the gradient elastic case, and particular in the cases $\lambda_A = \lambda_B = 0.2$ and $\lambda_A = 0.3, \lambda_B = 0.1$, the increase in not monotone and the solution oscillates, while increasing to the asymptotic limit. In all cases, for large values of the temporal variable, the gradient elasticity solution is of lower magnitude than that of the classical elasticity case. In particular, it is observed that as the microstructural parameter λ_B increases the material becomes stiffer.

The case $\mathrm{Bi} = \infty$ is more interesting. In this case, the temperature at $\xi = 0$ changes instantly form T_o to T_∞ at $\eta = 0$. For the classical elasticity case, since the traction $U_\xi - D_2\Theta$ at the free surface of the half-space is zero, the strain U_ξ features a finite jump at $\eta = 0$. The dashed black line for $\lambda_A = \lambda_B = 0$, corresponding to classical elasticity, presents this situation. The numerical solution features spurious oscillations which reduce in magnitude near this discontinuity at $\eta = 0$. In the gradient elastic case, where the zero traction condition at the free surface of the half-space is

$\lambda_A^2 U_{\xi\eta\eta} + U_\xi - \lambda_B^2 U_{\xi\xi\xi} - D_2\Theta = 0$, the strain is continuous despite the fact that the temperature features a discontinuity.

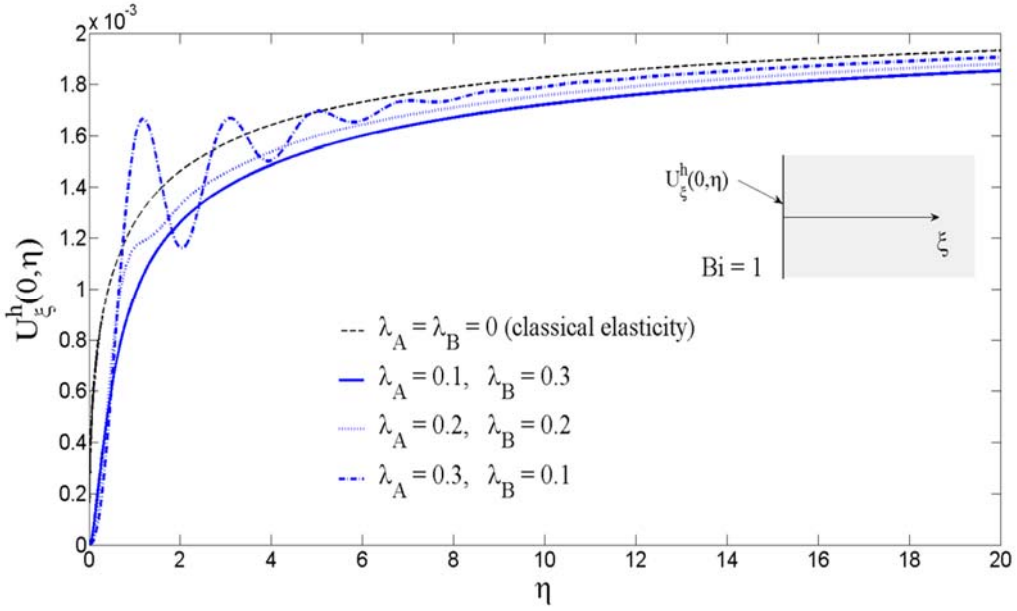

Figure 17. Displacement gradient at the free surface of the half-space as a function of time, for $\mathrm{Bi} = 1$.

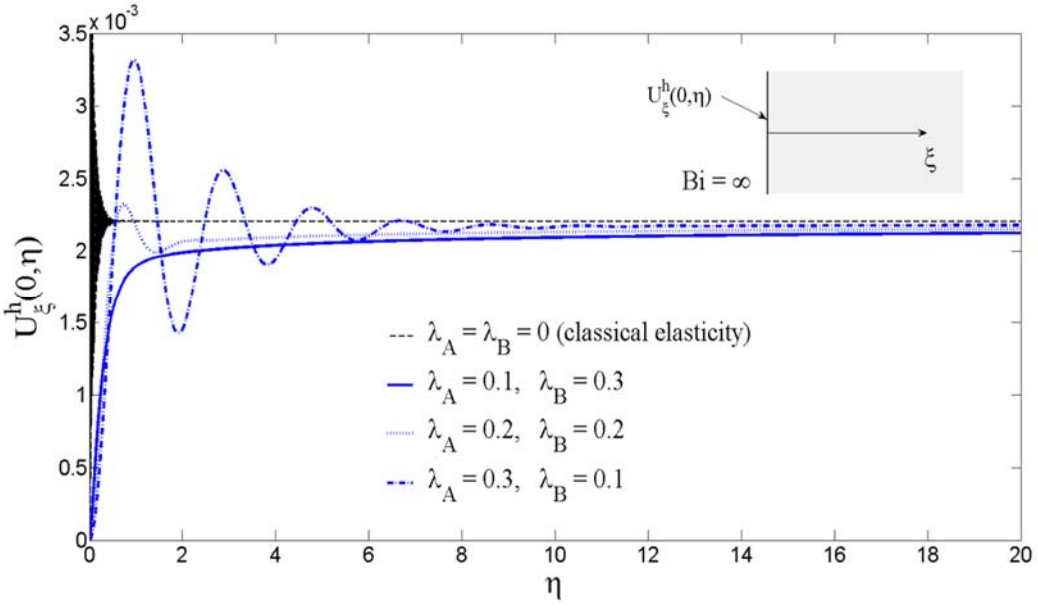

Figure 18. Displacement gradient at the free surface of the half-space as a function of time, for $\mathrm{Bi} = \infty$.

9. Conclusions

The thermal shock behavior of complex microstructured materials such as advanced ceramics, cellular materials, and foams is a problem of growing interest since their high performance properties are closely related to their reliability under changing thermal conditions. The present study extends the analysis of Danilovskaya [27, 28], where a thermal shock acts on a classical elastic half space, to a microstructured material modelled with gradient thermoelasticity. It is noted that due to the complexity of the equations of gradient thermoelasticity, very few solutions to benchmark initial-boundary value problems, such as the present one, exist in the literature. Special thermoelastic finite elements have been developed for the simulation of the response of a gradient elastic half-space subjected to thermal shock on its boundary. The Partial Differential Equations governing the phenomenon under consideration have been solved for different values of the microstructural parameters. The solution for a classical thermoelastic solid is obtained as a special case. Energy type stability estimates for the weak solution have been obtained for the fully coupled thermoelastic system as well as for the weakly coupled. The adopted finite element scheme performed well in all numerical experiments conducted. An important result obtained in the present study is that the displacement and strain fields induced by the thermoelastic shock are smoother (no kinks in displacements or discontinuities in strains) than the ones predicted by classical thermoelasticity. In addition, the thermoelastic pulse is of dispersive nature, as is typically the case for waves in gradient elastic solids. Normal or anomalous dispersion characteristics are observed depending on the values of the gradient parameters. Finally, we note that the differences between the solution of the fully coupled thermoelastic system and the weakly coupled have been found to be negligible for the material properties selected.

Acknowledgement: Theodosios K. Papathanasiou and Francesco Dal Corso gratefully acknowledge support from the European Union FP7 project "*Mechanics of refractory materials at high–temperature for advanced industrial technologies*" under contract number PIAPP–GA–2013–609758. Panos A. Gourgiotis gratefully acknowledges support from the ERC Advanced Grant "*Instabilities and nonlocal multiscale modelling of materials*" FP7-PEOPLE-IDEAS-ERC-2013-AdG (2014-2019).

References

1. G.A. Maugin, Generalized Continuum Mechanics: What do we mean by that?, in: G.A. Maugin, , A.V. Metrikine (Eds.), Mechanics of Generalized Continua. Springer, New York, (2010) 3-13.
2. P. Onck, E. Andrews, L. Gibson, Size effects in ductile cellular solids. Part I: Modeling. Int. J. Mech. Sci. 43 (2001) 681-699.

3. D. Bigoni, W.J. Drugan, Analytical derivation of Cosserat moduli via homogenization of heterogeneous elastic materials. ASME J. Appl. Mech. 74 (2007) 741-753.
4. R. Maranganti, P. Sharma, P., Length scales at which classical elasticity breaks down for various materials. Phys. Rev. Lett. 98 (2007) 195504.
5. M. Bacca, D. Bigoni, F. Dal Corso, D. Veber, Mindlin second-gradient elastic properties from dilute two-phase Cauchy-elastic composites Part I: Closed form expression for the effective higher-order constitutive tensor. Int. J. Solids Struct. 50 (2013) 4010-4019.
6. R. Lakes, Experimental micro-elasticity of two porous solids. Int. J. Solids Struct. 22 (1986) 55-63.
7. W. Anderson, R. Lakes, Size effects due to Cosserat elasticity and surface damage in closed-cell polymethacrylimide foam. J. Mater. Sci. 29, (1994) 6413-6419.
8. R. Lakes, Experimental methods for study of Cosserat elastic solids and other generalized elastic continua. in: H.B. Muhlhaus (Ed.), Continuum Models for Materials with Microstructure, John Wiley & Sons, Chichester (1995) 1-25.
9. H.G. Georgiadis, The mode-III crack problem in microstructured solids governed by dipolar gradient elasticity: Static and dynamic analysis, ASME J. Appl. Mech. 70 (2003) 517-530.
10. E. Radi, M. Gei, Mode III crack growth in linear hardening materials with strain gradient effects. Int. J. Fract. 130 (2004) 765-785.
11. P.A. Gourgiotis, A. Piccolroaz, Steady-state propagation of a Mode II crack in couple stress elasticity. Int. J. Fract. 188 (2014) 119-145.
12. Th. Zisis, P.A. Gourgiotis, K.P. Baxevanakis, H.G. Georgiadis, Some basic contact problems in couple-stress elasticity, Int. J. Solids Struct. 51 (2014) 2084-2095.
13. H. Mühlhaus., I. Vardoulakis, The thickness of shear bands in granular materials. Geotechnique 37 (1987) 271-283.
14. F. Dal Corso, F., J.R. Willis, Stability of strain gradient plastic materials. J. Mech. Phys. Solids 59 (2011) 1251-1267.
15. N.A. Fleck, J.W. Hutchinson, J.R. Willis, Strain gradient plasticity under non-proportional loading, Proc. Roy. Soc., A 470 (2014) 20140267.
16. R.A. Toupin, Elastic materials with couple-stresses. Arch. Ration. Mech. Anal. 11 (1962) 385-414.
17. R.D. Mindlin, Micro-structure in linear elasticity, Arch. Rat. Mech. Anal. 16 (1964) 51-78.
18. H.M Shodja, A. Zaheri, A. Tehranchi, Ab initio calculations of characteristic lengths of crystalline materials in first strain gradient elasticity. Mech. Mater. 61, (2013) 73-78.
19. D. Ieşan, Thermoelastic models of continua, Kluwer Academic Publishers, Dordrecht, 2004.
20. D. Ieşan, Thermoelasticity of non-simple materials, J. Therm. Stresses 12 (1989) 545-557.
21. R. Quintanilla, Thermoelasticity without energy dissipation of materials with microstructure, Appl. Math. Modelling 26 (2002) 1125-1137.

22. D. Ieşan, D., R. Quintanilla, On a strain gradient theory of thermoviscoelasticity. Mech. Res. Commun. 48 (2013) 52-58.
23. S.P. Filopoulos, T.K. Papathanasiou, S.I. Markolefas, G.J. Tsamasphyros, Generalized thermoelastic models for linear elastic materials with microstructure Part I: Enhanced Green-Lindsay model, J. Therm. Stresses 37 (2014) 624-641.
24. S.P. Filopoulos, T.K. Papathanasiou, S.I. Markolefas, G.J. Tsamasphyros, Generalized thermoelastic models for linear elastic materials with microstructure Part II: Enhanced Lord-Shulman model, J. Therm. Stresses 37 (2014) 642-659.
25. P. Vernotte, Les Paradoxes de la Theorie Continue de l' Equation de la Chaleur, C.R. Acad. Sci. (1958) 3154-3155.
26. C. Cattaneo, Sur un Forme de l' Equation de la Chaleur Eliminant le Paradox d'une Propagation Instantane´e, C. R. Acad. Sci. (1958) 431-432.
27. V.I. Danilovskaya: Thermal stresses in an elastic half-space arising after a sudden heating of its boundary, Prikl. Mat. Mekh. 14 (1950) 316-318.
28. V.I. Danilovskaya: On a dynamic problem of thermoelasticity, Prikl. Mat. Mekh. 16 (1952) 341-344.
29. R.B. Hetnarski, M. Reza Eslami, Thermal Stresses. Advanced theory and applications, Springer, 2009.
30. A.D. Kovalenko, Thermoelasticity. Basic theory and applications, Wolters-Noordhoff Publishing, Groningen, the Netherlands, 1969.
31. W. Nowacki, Dynamic Problems of Thermoelasticity, Noordhoff Int. Publishing, Leyden, the Netherlands, 1975.
32. S. Papargyri-Beskou, D. Polyzos, D.E. Beskos, Wave dispersion in gradient elastic solids and structures: a unified treatment. Int. J. Solids. Struct. 46 (2009) 3751–3759.
33. S.P. Filopoulos, T.K. Papathanasiou, S.I. Markolefas, G.J. Tsamasphyros, Dynamic finite element analysis of a gradient elastic bar with micro-inertia Comput. mech. 45 (2010) 311-319.
34. D.A. Fafalis, S.P. Filopoulos, G.J. Tsamasphyros, On the capability of generalized continuum to capture dispersion characteristics at the atomic scale, Eur. J. Mech. A:Solids 36 (2012) 25-37.
35. P.A. Gourgiotis, H.G. Georgiadis, I. Neocleous, On the reflection of waves in half-spaces of microstructured materials governed by dipolar gradient elasticity. Wave Motion 50 (2013) 437–455.
36. I. Vardoulakis, A. Giannakopoulos, An example of double forces taken from structural analysis. Int. J. Solids Struct. 43 (2006) 4047-4062.
37. W. Jaunzemis Continuum mechanics. New York, Macmillan, 1967.
38. M.E. Gurtin, E. Fried, L. Anand, The mechanics and thermodynamics of continua, Cambridge University Press, 2010.
39. H.G. Georgiadis, I. Vardoulakis, E.G. Velgaki, Dispersive Rayleigh-wave propagation in microstructured solids characterized by dipolar gradient elasticity. J. Elast. 74, (2004) 17-45.
40. H. Brezis, Functional analysis, Sobolev spaces and partial differential equations. Springer Science & Business Media, 2010.

41. R. Quintanilla, B. Straughan, Energy bounds for some non-standard problems in thermoelasticity. Proc. R. Soc. A 461 (2005) 1147-1162.
42. T.K. Papathanasiou, P.A. Gourgiotis, F. DalCorso and Th. Zisis, On the thermoelastic response of a gradient elastic half-space subjected to thermal shock on the boundary, 8th GRACM International Congress on Computational Mechanics, Volos, 12 July – 15 July 2015.
43. S. Jiang, Numerical solution for the Cauchy problem in nonlinear 1D thermoelasticity, Computing 44 (1990) 147-158.
44. T.K. Papathanasiou, A. Karperaki, E. E. Theotokoglou and K. A. Belibassakis, A higher-order FEM for time-domain hydroelastic analysis of large floating bodies in an inhomogeneous shallow water environment, Proc. R. Soc. A 471 (2015) 20140643.
45. P. Chadwick, Thermoelasticity: The dynamical theory. In: Sneddon, I.N., Hill, R. (Eds.), Progress in Solid Mechanics, vol. 1. North-Holland, Amsterdam, 1960.
46. A.C. Eringen, E.S. Suhubi, Elastodynamics, Vol. 1. Academic Press, New York, 1975.